Neutral Decay Modes of the η^0 Meson*

S. DEVONS, J. GRUNHAUS,† T. KOZLOWSKI, P. NEMETHY,‡ AND S. SHAPIRO§
Columbia University, New York, New York 10027

AND

N. HORWITZ, T. KALOGEROPOULOS, J. SKELLY, R. SMITH, AND H. UTO‖
Syracuse University, Syracuse, New York, 13210

(Received 24 November 1969)

The branching ratios of the decay of the η^0 meson into neutral products have been measured. The η^0 is produced in the reaction $\pi^-+p\rightarrow\eta^0+n$, and the decay products are observed as γ rays by a system of optical spark chambers and counters in nearly 4π geometry. Emphasis was placed on examining evidence for the decay mode $\eta^0\rightarrow\pi^0\gamma\gamma$ ($\rightarrow 4\gamma$). Measurement of the neutron time of flight in the production process, together with detailed measurement and kinematical analysis of the pictures showing four γ rays, enables us to test each event for consistency with such a decay mode, and also for the "background" process $\pi^-+p\rightarrow 2\pi^0+n$. From what is essentially a comparison of the observed rates for these processes, we obtain the upper limit for $(\eta^0\rightarrow\pi^0\gamma\gamma)/(\eta^0\rightarrow\text{all neutrals})\leq 7\%$ (90% confidence level), a result which is relatively insensitive to estimates of the efficiency of the detecting system. We also obtain $(\eta^0\rightarrow 3\pi^0)/(\eta^0\rightarrow 2\gamma)=0.75\pm 0.09$.

I. INTRODUCTION

MUCH experimental effort has been devoted in recent years to the study of the decay of the η^0 meson, and in particular to the identification and measurement of the more elusive neutral modes. In addition to the well-established charged modes $\pi^+\pi^-\pi^0$ and $\pi^+\pi^-\gamma$ and the neutral modes $3\pi^0$ and 2γ, there have been several reported observations of a significant partial decay rate for the mode $\pi^0\gamma\gamma$,[1] far larger than might have been theoretically expected.[2] On the other hand, some recent measurements yield only much smaller upper limits for this branching ratio.[3] Most of the reported measurements of the neutral decay modes are in reasonable agreement with respect to the ratio $(\eta^0\rightarrow 2\gamma)/(\eta^0\rightarrow\text{all neutral modes})$. An unexpectedly large value of $\eta^0\rightarrow\pi^0\gamma\gamma$ would then imply a reduced rate for $\eta^0\rightarrow 3\pi^0$, which in turn gives a smaller value for the ratio $(\eta^0\rightarrow 3\pi^0)/(\eta^0\rightarrow\pi^+\pi^-\pi^0)$,[4] one which is difficult to interpret on the basis of a plausible model of η decay. It is this possibility that has stimulated much of the theoretical speculation and interest in the neutral decay of the η^0 meson. Therefore, the main purpose of the experiment we report has been to make a careful check of the rate for the process $\eta^0\rightarrow\pi^0\gamma\gamma$.

The η^0 mesons were produced by means of the reaction $\pi^-+p\rightarrow\eta^0+n$ (π^- momentum approximately 860 MeV/c) with observation of the neutron in the forward direction. This method of production has been used in several other investigations of the η^0.[5] A major feature of this method is its enhancement of the neutron geometric detection efficiency. With this choice of π^- energy, observation of the neutron in the forward direction corresponds to production of η^0 approximately at rest, so that, essentially, all the original π^- momentum is transferred to the neutron. Under these conditions, neutron detectors subtend a solid angle in the center-of-mass system which is 9.4 times greater than that subtended in the laboratory system.

II. EXPERIMENTAL ARRANGEMENT

Figure 1 shows schematically the arrangement of our apparatus, details of which are described elsewhere.[6] A negative-pion beam (mean momentum 860 MeV/c, momentum spread $\Delta p/p=\pm\frac{1}{2}\%$) from the Brookhaven alternating gradient synchrotron (AGS), defined by the counter arrangement S_1S_2E, is incident on a liquid-hydrogen target (length $15\frac{1}{2}$ in., diam $5\frac{1}{2}$ in.). Apart from the hydrogen, there is less than 0.1 g/cm^2 of target material (Mylar end windows and superinsulation) in the beam path. The target is completely surrounded by anticounters A_1–A_5, which serve to eliminate from consideration events with charged particles in the final states.

* Research supported in part by the U. S. Atomic Energy Commission and the National Science Foundation.

† Present address: Tel Aviv University, Tel Aviv, Israel.

‡ Present address: Saclay, GIF Sur Yvette, France.

§ Present address: University of Rochester, Rochester, N. Y. 14627.

‖ Present address: Brookhaven National Laboratory, Upton, N. Y. 11973.

[1] G. DiGiugno, R. Querzoli, G. Truise, F. Vanoli, M. Giorgi, P. Schiavon, and V. Silvestrini, Phys. Rev. Letters **16**, 767 (1966); M. Feldman, W. Frati, R. Gleason, J. Halpern, M. Nussbaum, and S. Richtert, *ibid.* **18**, 868 (1967); J. Grunhaus (Ph.D. thesis), Nevis Laboratory Report No. 156, 1966 (unpublished); Z. S. Strugalski, I. V. Chuvilo, I. A. Ivanovska, L. S. Okhrimenko, B. Niczyporuk, T. Kanarek, B. Stowiuski, and Z. Jablonski, Report No. JINR-EI-3100, 1967 (unpublished).

[2] W. Alles, A. Baracca, and A. T. Ramos, Nuovo Cimento **45A**, 272 (1966).

[3] C. Baltay, in *Meson Spectroscopy*, edited by C. Baltay and A. H. Rosenfeld (Benjamin, New York, 1968), Chap. 7, p. 95.

[4] K. C. Wali, Phys. Rev. Letters **9**, 120 (1962).

[5] W. G. Jones, D. M. Binnie, A. Duane, J. P. Horsey, D. C. Mason, J. A. Newth, I. U. Rahman, J. Walters, N. Horwitz, and P. Palit, Phys. Letters **23**, 597 (1966); E. Hyman, W. Lee, J. Peoples, J. Schiff, C. Schultz, and S. Stein, Phys. Rev. **165**, 1437 (1968).

[6] S. Shapiro (Ph.D. thesis) Nevis Laboratory Report No. 174, 1969 (unpublished).

The whole target-counter array is surrounded on four sides by large stainless-steel γ-detecting spark chambers. Each chamber has 73 plates, 0.06 in. thick—a total thickness equivalent to about six radiation lengths. All four chambers are photographed in 90° stereo by a single camera placed high above the array. Figure 2 is a photograph of a typical four-γ event frame.

Above and below the target, as part of the detecting system and in those regions not covered by spark chambers, are located composite lead-glass–liquid-scintillator shower counters ($\check{C}_B$ and $\check{C}_T$). Each counter contains 21 sheets of 0.25-in.-thick lead glass (density $=4.88$ g/cm^3). The 0.5-in. space between the sheets is filled with a mineral-oil-base liquid scintillator, and the combination is viewed by five 5-in.-diam phototubes. The detection efficiency of these counters for 17-MeV γ rays (produced in the reaction $p+\mathrm{Li}^7 \rightarrow \mathrm{Be}^8+\gamma$) was measured to be better than 90%. The over-all detection efficiency (conversion efficiency×percentage of sphere covered) of the counters and of the spark chambers as a function of incident γ-ray energy is illustrated in Fig. 3. The combined spark-chamber–shower-counter

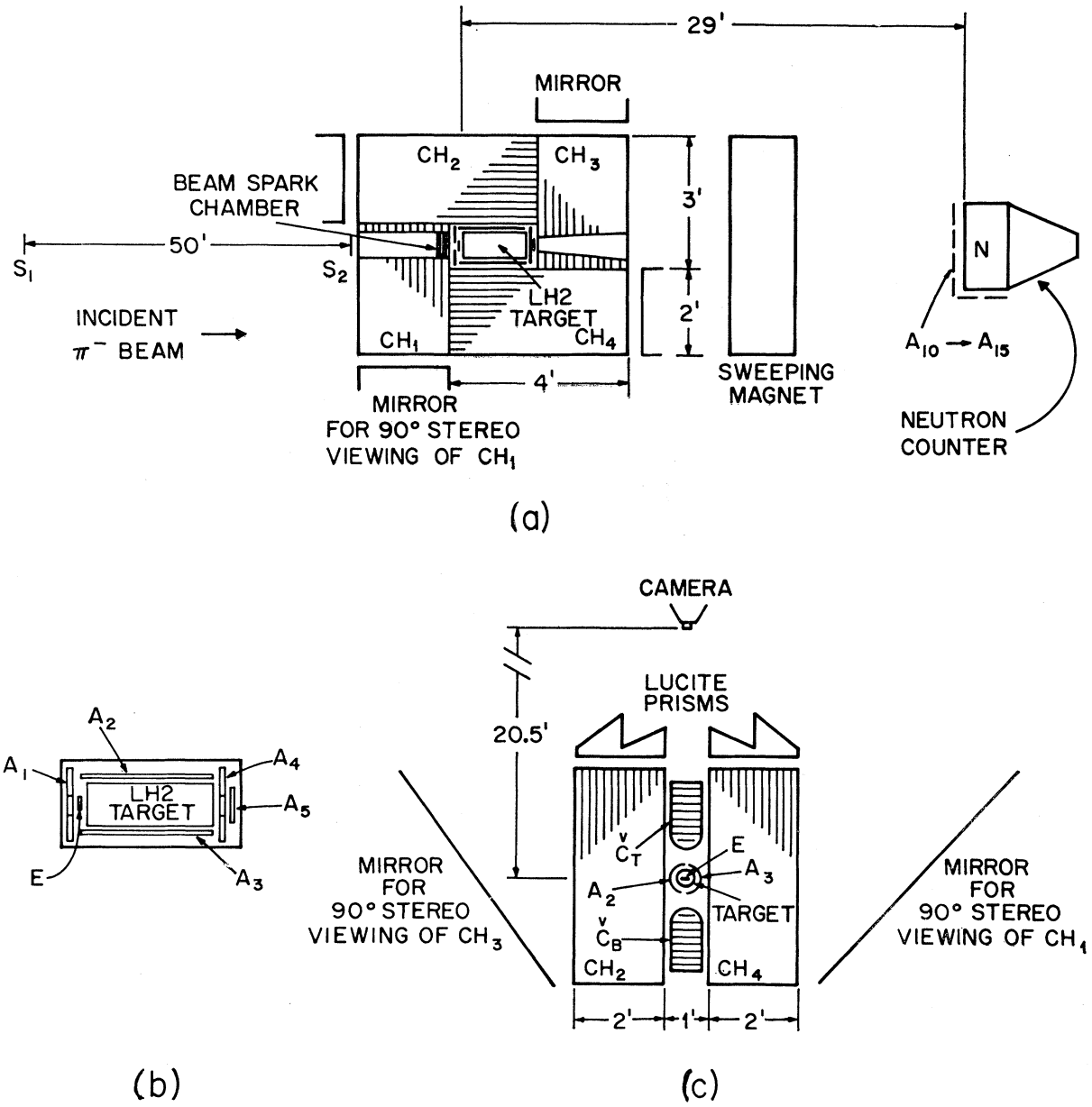

FIG. 1. (a) Schematic of the experimental arrangement (plan view). The counters labeled A are operated in anticoincidence; $\check{C}_T$ and $\check{C}_B$ are lead glass Čerenkov counters. (b) Close-up of the target region. (c) Schematic of the experimental arrangement as seen by the incident π^-.

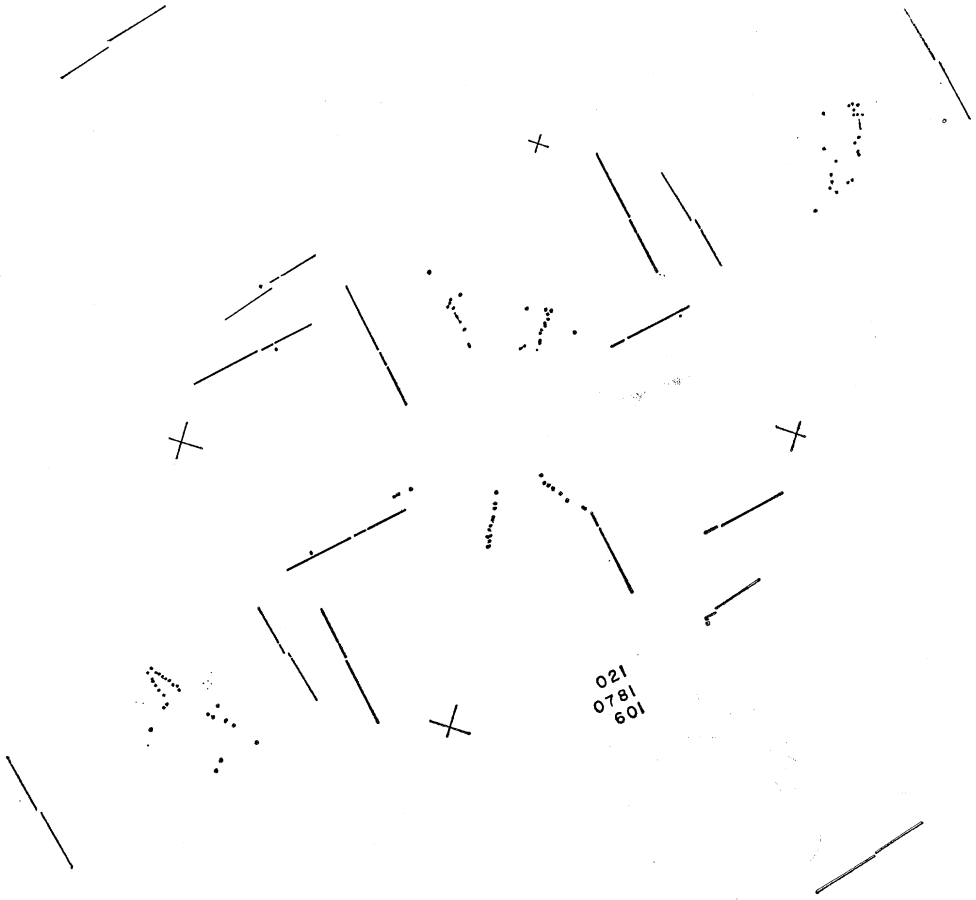

FIG. 2. Typical four-γ-event photograph. (The π^- beam enters from the left.)

array covers about 90% of the sphere around the target center.

The upstream spark chamber, which is traversed by the π^- beam before it reaches the target, is modified to include within it a thin foil chamber, which records accurately the direction and location of the incident pions. The plates of the downstream chamber are modified so as to provide a divergent conical tunnel with its axis along the beam, through which neutrons produced in the forward direction can pass unhindered. (The holes in the steel plates which form this tunnel are covered with Mylar foil.) Beyond this chamber, a large sweeping magnet moves charged particles out of the beam direction.

The neutrons in the forward direction are detected by a 2-ft-square×1-ft-deep liquid scintillation counter: an aluminum box, centered on the beam line, filled with Toluene-PPO-POPOP scintillator, screened (from charged particles) by the anticounters A_{10}–A_{15}. It is located 28 ft downstream of the hydrogen-target center, so that the mean angle of detection of the neutrons, with respect to the incident pions, is about 1°. The neutron counter intercepts 0.9% of the neutrons produced in the forward center-of-mass hemisphere of the reaction $\pi^-+p\rightarrow\eta^0+n$. These forward neutrons have a mean kinetic energy of 320 MeV, corresponding to a flight time of 43.5 nsec. The scintillation detector is biased so as to record an energy loss greater than about 50 MeV. A neutron time-of-flight spectrum in the region of the η^0 peak is shown in Fig. 4(a).

In operation, events are initiated by the arrival of a beam pion in the target with no accompanying pulses in the surrounding counters (i.e., $S_1S_2E\bar{A}_1\cdots\bar{A}_5$). If a fast neutron pulse occurs in a predetermined time interval after the pion (in practice, usually 37.5–52 nsec), the spark chambers are fired, and photographs of the γ showers are taken. Also recorded for each event are (i) the neutron time of flight (TOF) (digitized and recorded on film); (ii) signals, if any, from the shower counters; and (iii) monitor signals from each of 28 spark gaps operating the spark chambers to check efficient operation (i.e., firing within 60 nsec of the triggering pulse). Figure 4(b) is the neutron TOF spectrum recorded for a sample of the events which were photographed.

Most of the measurements were made with an incident pion beam intensity of 2×10^5 pions per pulse (an average rate during the spill of 8×10^5 pions per second).

About 1% of the entering pions started a time sequence and, of these, some 0.03% were accompanied by a recorded neutron, and, therefore, a spark chamber "event." In all, some 25 000 "events" were recorded.

III. ANALYSIS

Our data are a sample from events of the type $\pi^-+p\rightarrow n+$ (neutral products), in which n is an energetic neutron near 0°. The peak in the neutron TOF spectrum, at 565 channels in Fig. 4(b), corresponds to the 2-body reaction $\pi^-+p\rightarrow\eta^0+n$. The background is due chiefly to $\pi^-+p\rightarrow n+2\pi^0$ and $\pi^-+p\rightarrow n+3\pi^0$, for which the neutron energy is not well defined.

The 2γ, $\pi^0\gamma\gamma$, and $3\pi^0$ neutral decay modes of the η^0 result in 2, 4, and 6 γ rays, respectively, so that with 100% detection efficiency, these different modes could be distinguished by simply counting the number of γ rays. (One would, of course, need to guard against events caused by more than one entering pion, which, in our arrangement, is possible by observation of the pion beam tracks.) With the actual imperfect detection efficiency, one can still attempt to relate the distribution of decay modes according to the observed distribution of γ-ray multiplicities, provided the efficiency for detection of γ rays is well known. However, although this method of analysis has been used in some investigations, it is, for multi-γ-ray events, notoriously dependent on precise knowledge of the detection efficiency. Since this efficiency must be known for a wide range of γ energies and all parts of the detection array, it is difficult to be sure of the reliability of such a procedure. This is especially true of attempts to measure the rate of a four-γ process ($\pi^0\gamma\gamma$) in the presence of a large six-γ background process (viz., $3\pi^0$ decay). For the examination of the $\pi^0\gamma\gamma$ process, we have, therefore, used a method of analysis which does not depend so heavily on the assessment of γ-detection efficiency.

Our γ-ray detection system provides reasonably good angular resolution for detected γ rays. The γ-ray directions, together with a knowledge of incoming pion and outgoing neutron momenta, permit a kinematical reconstruction of all pictures showing four γ rays. These might then be $\eta^0\rightarrow\pi^0\gamma\gamma$—events in which more than four γ rays are produced but only four are detected—or $\pi^-+p\rightarrow n+2\pi^0$ events. This last is a major source of four-γ events which form a "background" of possible confusion with the $\pi^0\gamma\gamma$ events, but it also provides a means of checking the sensitivity of the detection system. The kinematical analysis allows these three categories of events to be distinguished from each other.

The most straightforward determination of the desired branching ratio, $R\equiv(\eta^0\rightarrow\pi^0\gamma\gamma)/(\eta^0\rightarrow$ all neutrals), would be obtained from the relation

$$M_{\rm obs}(\pi^0\gamma\gamma)=N(\eta)R\epsilon(\pi^0\gamma\gamma)+M_{\rm BGD}(\pi^0\gamma\gamma), \quad (1)$$

where $M_{\rm obs}(\pi^0\gamma\gamma)$ is the observed number of kinematically identified $\eta^0\rightarrow\pi^0\gamma\gamma$ events, $M_{\rm BGD}(\pi^0\gamma\gamma)$ is the calculated number of NON-$(\eta^0\rightarrow\pi^0\gamma\gamma)$ events which simulate real $\eta^0\rightarrow\pi^0\gamma\gamma$ events, $N(\eta)$ is the number of neutral-decaying η^0's produced which are associated with the detected fast neutron, and $\epsilon(\pi^0\gamma\gamma)$ is the overall efficiency for the detection and identification of an $\eta^0\rightarrow\pi^0\gamma\gamma$ event. However, $\epsilon(\pi^0\gamma\gamma)$ is difficult to estimate, especially that part which gives the fraction of *real* $\eta^0\rightarrow\pi^0\gamma\gamma$ that satisfies the rather severe kinematical criteria used to discriminate against background events. For this reason, the value of R is derived more reliably from a comparison of the observed rates of $\eta^0\rightarrow\pi^0\gamma\gamma$ in the "η^0-peak" region and $\pi^-+p\rightarrow n+2\pi^0$ in the "off-peak" regions (as defined in Sec. III A). Analogous to Eq. (1), we have

$$M^*_{\rm obs}(2\pi^0)=N^*(2\pi^0)\epsilon^*(2\pi^0)+M^*_{\rm BGD}(2\pi^0), \quad (2)$$

where the asterisk means that the quantity refers to events with neutron TOF in the off-peak regions only. $M^*_{\rm obs}(2\pi^0)$, $M^*_{\rm BGD}(2\pi^0)$, $N^*(2\pi^0)$, and $\epsilon^*(2\pi^0)$ are defined analogously to similar quantities in Eq. (1). For

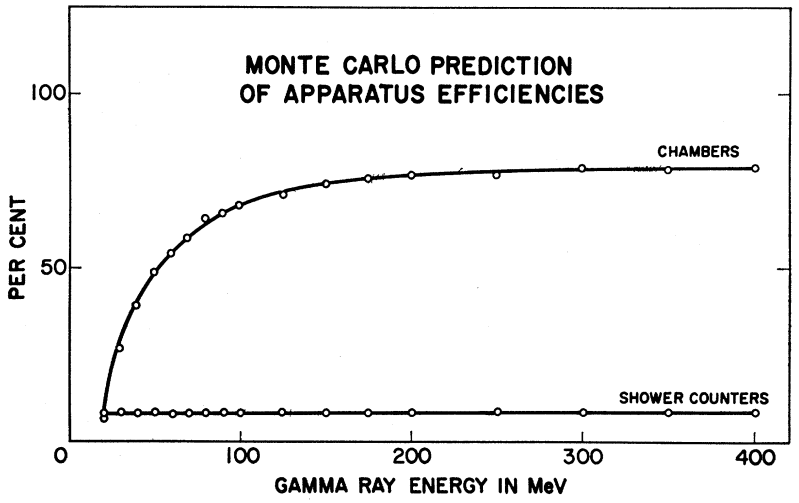

FIG. 3. Monte Carlo predictions of apparatus detection efficiency showing separately the efficiency of the chambers and shower counters.

example, $N^*(2\pi^0)$ is the number of $\pi^-+p\rightarrow n+2\pi^0$ reactions with neutron TOF in the off-peak region.

Dividing Eq. (1) by Eq. (2), we have

$$\frac{M_{\rm obs}(\pi^0\gamma\gamma)}{M^*_{\rm obs}(2\pi^0)}=\frac{N(\eta)R\epsilon(\pi^0\gamma\gamma)+M_{\rm BGD}(\pi^0\gamma\gamma)}{N^*(2\pi^0)\epsilon^*(2\pi^0)+M^*_{\rm BGD}(2\pi^0)}. \quad (3)$$

To see the merit of Eq. (3), assume the background-correction terms $M_{\rm BGD}(\pi^0\gamma\gamma)$ and $M^*_{\rm BGD}(2\pi^0)$ are zero. Then R depends on the *ratio* of the calculated efficiencies $\epsilon(\pi^0\gamma\gamma)/\epsilon^*(2\pi^0)$. Since the two final states $2\pi^0$ and $\pi^0\gamma\gamma$ involve the same number of γ rays and similar total energy, we expect

$$\epsilon(\pi^0\gamma\gamma)/\epsilon^*(2\pi^0)\approx 1. \quad (4)$$

Thus R obtained from Eq. (3) would not depend as strongly on a Monte Carlo calculation of efficiencies as the R calculated from Eq. (1). This conclusion is weakened, somewhat, when the background terms are considered; but, as explained in Sec. III E, R determined from Eq. (3) is still less Monte Carlo dependent than R determined from Eq. (1).

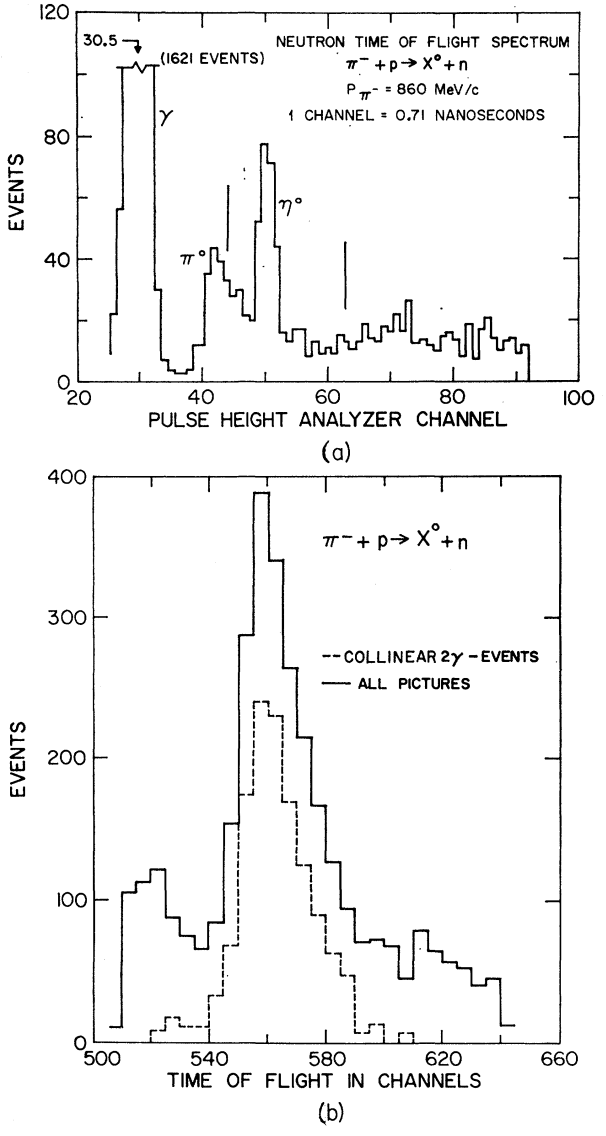

FIG. 4. (a) Neutron time-of-flight histogram of the entire spectrum as observed and recorded on a 100-channel analyzer. The vertical bars indicate the region in which data are taken. (b) Neutron time-of-flight spectrum taken from a fraction of our data film. All one–six-γ events showing no chamber malfunction and no double beam tracks are included. The dashed histogram is the neutron time-of-flight spectrum of collinear two-γ events only, and as such defines the η-peak position. The time-of-flight values (horizontal scale) are those which appear on the film.

A. Definition of Neutron Time-of-Flight Regions

In the neutron TOF spectrum [Fig. 4(b)], we separate the events into two categories: (1) those where the observed neutron has a momentum near the value appropriate to η^0 production (the "η^0 peak"), and (2) the events corresponding to multiparticle reactions, $\pi^-+p\rightarrow n+2\pi^0$, etc., in regions where η^0 production is negligible (the "off peak"). The "η peak" is defined as the region between channels 550 and 580 [Fig. 4(b)], corresponding to the TOF between 42.7 and 44.8 nsec. The off-peak region is defined as channels 510–550 and 580–640 [Fig. 4(b)]. In the η^0-peak region, most of the events are attributable to η^0 decays with some admixture of background processes. In the off-peak region there is negligible contribution from η^0 production, and the process of major importance is $\pi^-+p\rightarrow n+2\pi^0$. The location of the η^0 peak can be found reliably and unambiguously by recording the neutron TOF for all events showing two and only two high-energy collinear γ rays (with no γ ray detected by the shower counters). These events are the decays (at rest) of η^0 into two γ rays. The TOF distribution of these events is also shown in Fig. 4(b) (dashed line).

B. Kinematic Analysis of Four-γ Events (to Determine $M_{\rm obs}$'s)

We analyze all four-γ events for kinematical consistency with the modes $\eta^0\rightarrow\pi^0\gamma\gamma$ and $\pi^-+p\rightarrow n+2\pi^0$.

To test a four-γ event for compatibility with the reaction $\pi^-+p\rightarrow n+2\pi^0$, we analyze each four-$\gamma$ event as follows: The incoming π^- momentum and neutron TOF serve to fix the invariant mass and momentum of the four-γ system. This, combined with the eight measured angles and the conservation laws, yields the four-γ energies and so determines the kinematics completely. That is to say, we do a zero-constraint fit (there is no quadratic ambiguity for γ rays) and retain solutions in which all four energies are real and positive. There are three different ways to pair the four γ rays. For each pairing combination we calculate the invariant mass of both γ-ray pairs. These masses are plotted in Fig. 5(a). The clustering of points at $2\pi^0$ masses is clear, and the indicated mass resolution is approximately ± 20 MeV. We therefore adopt as a first criterion of $2\pi^0$

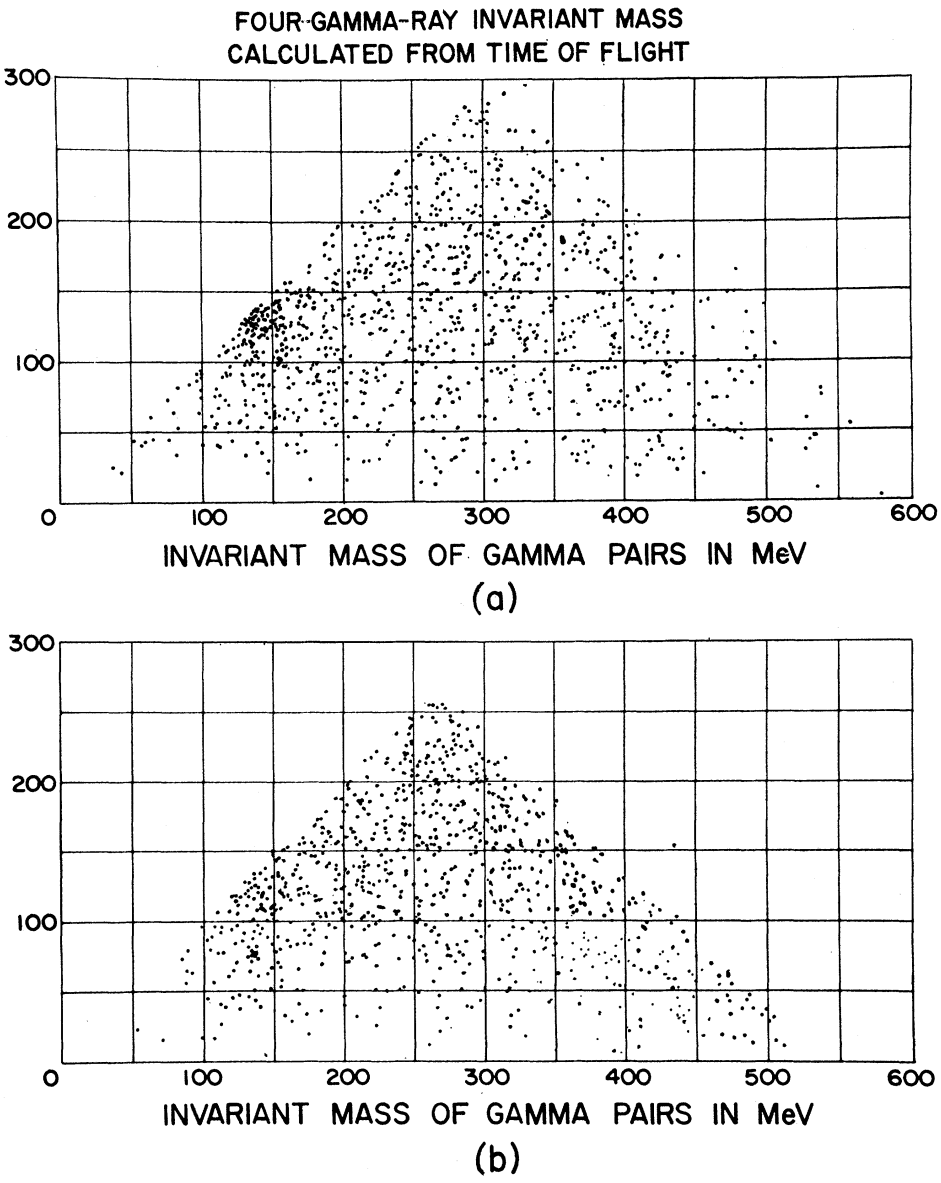

FIG. 5. Both scatter plots contain three points per event reflecting the three pairing combinations. (a) The invariant mass of the four-γ system is determined by the use of the neutron time-of-flight information (237 events). (b) The invariant mass of the four-γ system is chosen to be the η^0 mass 548.9 MeV (193 events).

compatibility the requirement that some pairing combination results in two invariant masses, each of which is in the interval 135 ± 20 MeV.

The procedure for the $\eta^0 \to \pi^0\gamma\gamma$ test differs in that for events with TOF in the η^0 peak, the exact value of the TOF is ignored and, instead, the invariant mass of the four γ rays is assumed to be the η^0 mass. As before, we do a zero-constraint fit and retain solutions in which the four energies are real and positive. The resultant $\gamma\gamma$ invariant masses are displayed in Fig. 5(b). The square of the matrix element for the decay $\eta^0 \to \pi^0\gamma\gamma$ is assumed proportional to $m_{\gamma\gamma}{}^4$ when $m_{\gamma\gamma}$ is the invariant mass of the two γ rays.[7] The resultant distribution is such that $m_{\gamma\gamma}>200$ MeV for 97% of the decays. We therefore adopt as our first criterion for $\pi^0\gamma\gamma$ compatibility the requirement that some pairing combination of the four γ rays result in one invariant mass within the interval 135 ± 20 MeV and the other invariant mass be greater than 200 MeV.

[7] The simplest gauge-invariant matrix element for this decay is $M=(\epsilon_1\cdot\epsilon_2)(k_1\cdot k_2)-(\epsilon_1\cdot k_2)(\epsilon_2\cdot k_1)$, where ϵ and k are the polarization and momentum vectors of the photons. After squaring and summing over final-state polarizations, we obtain the aforementioned result. This matrix element and others are discussed by K. Hiida, Y. Y. Lee, and T. Sakuma, Phys. Rev. 161, 1428 (1967).

TABLE I. Predicted γ-ray multiplicities for 40 000 events.

Channel	Total[a] triggers	Number of γ rays observed with no shower-counter signal: 0 γ	1 γ	2 γ	3 γ	4 γ	5 γ	6 γ	Total triggers with no shower-counter signal
$\pi^-+p\rightarrow\pi^0+n$	34 968	2704	13 592	17 536	...	...	...	...	33 822
$\eta^0\rightarrow 2\gamma$	36 384	1168	5 432	25 536	...	...	...	...	32 136
$\eta^0\rightarrow\pi^0\gamma\gamma$	32 864	67	887	4 701	10 787	7677	...	...	24 119
$\pi^-+p\rightarrow 2\pi^0+n$	32 773	118	1 162	5 665	10 666	6708	...	...	24 319
$\eta^0\rightarrow 3\pi^0$	29 923	13	179	1 236	3 778	6211	5333	1636	18 386
$\pi^-+p\rightarrow 3\pi^0+n$	29 864	16	64	856	3 032	5904	6552	2736	19 160

[a] The difference between 40 000 and the number of "total triggers" is the number of events in which a γ ray has converted in the target region and the resulting charged particle has been detected by A_1–A_5. These events will not trigger the chambers.

In addition, we impose on each event the following criteria:

(i) Every reconstructed vertex must be within the target fiducial volume.

(ii) All the γ rays of an event must point back to a single vertex point with an accuracy consistent with our estimate of angular resolution. (For single γ-ray showers, the angular resolution in space is 14.5°.)

(iii) The number of sparks observed for each γ-ray shower must be consistent, within error, with the number predicted using the energy calculated in the kinematical analysis (spark resolution $\Delta N/N=0.45$ for $E_\gamma\approx 150$ MeV [8]).

C. Monte Carlo Calculation (to Determine ϵ's)

The effect of the above selection criteria is, of course, to exclude a large proportion of the real events (as well as four-γ events arising from other processes), and it is this factor, together with the probability of the γ rays being detected, that determines the efficiency. There is a further factor to be included in the over-all efficiency: In addition to the factors that can be estimated and that are included in the Monte Carlo calculation described below, a small proportion of the event pictures is unsuitable for kinematical analysis (missing sparks, tracks obscured by miscellaneous parts of the apparatus, etc.). This factor is determined empirically from the examination of all the four-γ events and is included in the calculated over-all efficiencies.

In order to calculate $M_{\mathrm{BGD}}(\pi^0\gamma\gamma)$ and $M^*{}_{\mathrm{BDG}}(2\pi^0)$, we need the probability of misidentification of events due to our finite angular resolution. Thus we must calculate various $\epsilon_I(J)$, defined to be the probability that an event of type I is identified as an event of type J. This is particularly important if the $\pi^0\gamma\gamma$ rate is small, because it could be seriously confused with a contribution $M_{\mathrm{BGD}}(\pi^0\gamma\gamma)$ from background $2\pi^0$ events or incompletely detected $3\pi^0$ events. The Monte Carlo calculation of the ϵ's was done as follows.

First, we considered all relevant neutral processes, i.e., η^0 decays to 2γ, $\pi^0\gamma\gamma$, and $3\pi^0$ and production of π^0, $2\pi^0$, and $3\pi^0$, and estimated for each process the probability of observing one, two, ..., six γ-ray showers. For the $2\pi^0$ events we assume the π^0's to be emitted isotropically in the $\pi^0\pi^0$ center-of-mass system; for the $\eta^0\rightarrow\pi^0\gamma\gamma$ we assume over-all isotropy and use the matrix element mentioned earlier, viz., $m_{\gamma\gamma}{}^4$. For each γ ray of each process, we consider the probability of its conversion in the hydrogen target, the target walls, and anticounters, and the probability that it produces a visible shower in the steel plates of the spark chamber or in the shower counter. All these processes are functions of the energy and direction of the γ rays. Table I tabulates the results of this program.

For those events which yield four detected γ showers, we introduce angle errors and spark count and then follow those events through vertex and kinematics routines including all cuts and restrictions present in the analysis of our actual data. The resulting over-all efficiencies are tabluated in Table II.

D. γ-Multiplicity Fitting (to Determine N's)

We next determine the abundances of the various processes—in particular, the number of η^0's in the peak and the number of $2\pi^0$'s in the off peak by a fitting program. We use here only the first part of the Monte Carlo calculations, i.e., the part concerned with detection efficiency, but not with detailed kinematics. The detection efficiencies given by these calculations are taken as fixed parameters. We take as variables $N_{(\eta)}$,

TABLE II. Over-all efficiencies [see text for definitions of ϵ's and $\epsilon_I(J)$].

$\epsilon(\pi^0\gamma\gamma)$	0.0273
$\epsilon_{2\pi}(\pi^0\gamma\gamma)$	0.0101
$\epsilon_{3\pi}(\pi^0\gamma\gamma)$	0.0023
$\epsilon(2\pi^0)$	0.0181
$\epsilon^*(2\pi^0)$	0.0216
$\epsilon^*{}_{3\pi}(2\pi^0)$	0.0002
$\epsilon^*{}_{2\pi}(\pi^0\gamma\gamma)$	0.0108
$\epsilon^*{}_{3\pi}(\pi^0\gamma\gamma)$	0.0024

[8] The number of sparks in each γ-ray shower is first adjusted to account for the angle that the γ ray makes with the normal to to the chamber plates. To get the spark-count-to-energy calibration, we use our sample of observed, kinematically valid $2\pi^0$ events (60 in all) and our sample of collinear two-γ events (140 in all). Each pair of numbers (energy, corrected spark count) is used as input to a least-squares fitting routine. The results are as follows: sparks $=0.627E_\gamma-0.761\times10^{-2}E_\gamma{}^2+0.364\times10^{-4}E_\gamma{}^3-0.559\times10^{-7}E_\gamma{}^4$, and $\sigma_{\mathrm{spk}}(E_\gamma)=(0.59-0.0009E_\gamma)\times$(sparks), for E_γ in the energy region 0–300 MeV.

TABLE III. Comparison of observed and (fitted) γ-ray multiplicities. These data were obtained from a sample of roughly half of our event frames. Only single beam track events for which the chambers appear to have worked perfectly are included. The presence of shower counter lights is ignored.

Region (channels) \ Number of γ rays	1	2	3	4	5	6	All
$510 \leq \text{TOF} \leq 540$	104(129)	202(180)	136(131)	83(86)	24(26)	8(6)	557(556)
$541 \leq \text{TOF} \leq 590$	245(294)	909(874)	399(371)	315(356)	198(197)	71(48)	2137(2140)
$591 \leq \text{TOF} \leq 640$	106(103)	192(165)	152(178)	105(118)	43(40)	14(12)	612(616)

$N_{(\pi)}, N_{(2\pi)}, N_{(3\pi)}, N_{\text{non-H}}; N'_{(\pi)}, N'_{(2\pi)}, N'_{(3\pi)}, N'_{\text{non-H}}; N''_{(\pi)}, N''_{(2\pi)}, N''_{(3\pi)}$, and $N''_{\text{non-H}}$. $N_{(\eta)}$ is the number of (neutrally decaying) η's in the peak. $N_{(\pi)}$, $N_{(2\pi)}$, and $N_{(3\pi)}$ are the number of $n\pi^0$-producing reactions in this same region. $N'_{(\pi)}$, $N'_{(2\pi)}$, $N'_{(3\pi)}$, $N''_{(\pi)}$, $N''_{(2\pi)}$, and $N''_{(3\pi)}$ are the corresponding numbers for the off-peak regions, channels 510–550 and 580–640

$$[N^*(2\pi)=N'(2\pi)+N''(2\pi), \text{ etc.}].$$

$N_{\text{non-H}}$ is background due to materials other than hydrogen.

With the above variables, we seek a fit to (1) the observed number of one-, two-, ..., six-γ shower events associated with each neutron TOF region, (2) the shape of the TOF spectrum for $2\pi^0$ events, (3) the shape of the TOF spectrum of the non-hydrogen background and the absolute rate (data were obtained from target-empty runs), and (4) the $\pi^-+p \to n+\pi^0$ absolute rate. In this program, we assume the value 0.57 for the ratio $R_{2\gamma}=(\eta^0 \to 2\gamma)/(\eta^0 \to \text{all neutrals})$. The ratio $R=(\eta^0 \to \pi^0\gamma\gamma)/(\eta^0 \to \text{all neutrals})$ is first assumed to be zero and then 0.1. The difference between these two assumptions is, as we expected, quite negligible as far as the values of the N's are concerned. If the efficiencies calculated by the Monte Carlo program are correct, then there should be some choice of the N's which will produce a good fit. The quality of the agreement between the observed and calculated γ-ray multiplicities for the optimum values of the N's is shown in Table III. The optimum values of the N's are tabulated in Table IV.

After the rate for $\eta^0 \to \pi^0\gamma\gamma$ has been established from the detailed kinematical analysis of four-γ events, we can again compare the predicted and observed γ multiplicities to reestablish the rates for the dominant modes $\eta^0 \to 3\pi^0$ and $\eta^0 \to 2\gamma$ in the peak, and $2\pi^0$, $3\pi^0$ production in the off-peak region.

TABLE IV. Optimum numbers "N_I" in each reaction channel.

Region (channels) \ Channel	N_π	$N_{2\pi}$	$N_{3\pi}$	N_η	$N_{\text{non-H}}$
$510 \leq \text{TOF} \leq 550$	221	612	321	298	414
$551 \leq \text{TOF} \leq 580$	0	478	236	2987	278
$581 \leq \text{TOF} \leq 640$	0	894	427	298	467

E. Estimate of Background (to Determine M_{BDG}'s)

The Monte Carlo simulation of the kinematical analysis is of critical importance in estimating the number of other events which kinematically simulate the $\pi^0\gamma\gamma$ process—in particular, the contribution from $\eta^0 \to 3\pi^0$ and from the $2\pi^0$ and $3\pi^0$ backgrounds under the η peak. Specifically, these corrections are

$$M_{\text{BGD}}(\pi^0\gamma\gamma)=N_{(\eta)}R_{3\pi}\epsilon_{3\pi}(\pi^0\gamma\gamma) + N(2\pi)\epsilon_{2\pi}(\pi^0\gamma\gamma)+N(3\pi)\epsilon_{3\pi}(\pi^0\gamma\gamma), \quad (5)$$

where $R_{3\pi}=1-R_{2\gamma}-R$. To illustrate the magnitude of the various background contributions, assume $R_{3\pi}=0.43$ and use the numbers in Tables II and IV to find

$$N_{(\eta)}R_{3\pi}\epsilon_{3\pi}(\pi^0\gamma\gamma)=3.0,$$
$$N_{(2\pi^0)}\epsilon_{2\pi}(\pi^0\gamma\gamma)=4.8,$$
$$N_{(3\pi^0)}\epsilon_{3\pi}(\pi^0\gamma\gamma)=0.5.$$

Thus the calculated value of $M_{\text{BGD}}(\pi^0\gamma\gamma)$ is 8.3 events. We see that the contribution to $M_{\text{BGD}}(\pi^0\gamma\gamma)$ from the $\pi^-+p \to n+3\pi^0$ channel is relatively unimportant. The contribution from this channel to the denominator of Eq. (3) is even less significant,

$$N^*_{(3\pi^0)}\epsilon^*_{3\pi}(2\pi^0)/N^*_{(2\pi^0)})\epsilon^*(2\pi^0)=0.004,$$

and both of these terms will be ignored in what follows to simplify the discussion. Using this simplification and substituting Eq. (5) into Eq. (3), we get

$$\frac{M_{\text{obs}}(\pi^0\gamma\gamma)}{M^*_{\text{obs}}(2\pi^0)} = \frac{N_{(\eta)}R\epsilon(\pi^0\gamma\gamma)}{N^*_{(2\pi^0)}\epsilon^*(2\pi^0)} + \frac{N_{(\eta)}R_{3\pi}\epsilon_{3\pi}(\pi^0\gamma\gamma)}{N^*_{(2\pi^0)}\epsilon^*(2\pi^0)} + \frac{N_{(2\pi^0)}\epsilon_{2\pi}(\pi^0\gamma\gamma)}{N^*_{(2\pi^0)}\epsilon^*(2\pi^0)}. \quad (6)$$

As mentioned earlier, and as is clear from Eq. (6), if $M_{\text{BGD}}(\pi^0\gamma\gamma)$ is zero, then R depends on the ratio $\epsilon(\pi^0\gamma\gamma)/\epsilon^*(2\pi^0)$. Even if $M_{\text{BGD}}(\pi^0\gamma\gamma)$ is not zero, Eq. (6) shows that R is modified by terms which only depend on ratios of efficiencies, i.e., $\epsilon_{2\pi}(\pi^0\gamma\gamma)/\epsilon^*(2\pi^0)$ and $\epsilon_{3\pi}(\pi^0\gamma\gamma)/\epsilon^*(2\pi^0)$. These ratios are not expected to be of order unity, however; owing to the cancellation of common factors, we expect the ratios to be more reliable than the individual ϵ's.

A reliable determination of $M_{\mathrm{BGD}}(\pi^0\gamma\gamma)$ is important because, as will be seen (Sec. IV), the calculated background more than accounts for the number of observed events $M_{\mathrm{obs}}(\pi^0\gamma\gamma)$. The biggest background contribution [the last term in Eq. (6)] arises from the $\pi^-+p\rightarrow n+2\pi^0$ channel. We can estimate this contribution in a way that is insensitive to the Monte Carlo calculations.

In the off-peak region we observed a number of events $M^*_{\mathrm{obs}}(\pi^0\gamma\gamma)$ which could be fitted to the scheme $\pi^-+p\rightarrow n+X^0$, $X^0\rightarrow\pi^0\gamma\gamma$, for which X^0 must obviously have an invariant mass different from the η^0. These spurious events arose from errors in detection and measurement of $2\pi^0$ and $3\pi^0$ processes (non-hydrogen events are negligible). These same errors will also give rise to similar spurious events from these channels under the η peak, but here with the correct mass. It is precisely these events, along with those from $\eta^0\rightarrow 3\pi^0$, which constitute $M_{\mathrm{BGD}}(\pi^0\gamma\gamma)$. We are able to use the measured value $M^*_{\mathrm{obs}}(\pi^0\gamma\gamma)$ as follows.

Let $T_{2\pi}$ be the last term in Eq. (6):

$$T_{2\pi}=\frac{N_{(2\pi)}\epsilon_{2\pi}(\pi^0\gamma\gamma)}{N^*_{(2\pi)}\epsilon^*_{(2\pi^0)}}. \tag{7}$$

We also have

$$\frac{M_{\mathrm{obs}}(2\pi^0)}{M^*_{\mathrm{obs}}(2\pi^0)}=\frac{N_{(2\pi)}\epsilon(2\pi)}{N^*_{(2\pi)}\epsilon^*(2\pi)} \tag{8}$$

and

$$\frac{M^*_{\mathrm{obs}}(\pi^0\gamma\gamma)}{M^*_{\mathrm{obs}}(2\pi^0)}=\frac{N^*_{(2\pi)}\epsilon^*_{2\pi}(\pi^0\gamma\gamma)+N^*_{(3\pi)}\epsilon^*_{3\pi}(\pi^0\gamma\gamma)}{N^*_{(2\pi)}\epsilon^*(2\pi)}, \tag{9}$$

$$N^*_{(3\pi)}\epsilon^*_{3\pi}(\pi^0\gamma\gamma)\ll N^*_{(2\pi)}\epsilon^*_{2\pi}(\pi^0\gamma\gamma). \tag{10}$$

Combining Eqs. (7)–(10),

$$T_{2\pi}=\frac{M_{\mathrm{obs}}(2\pi)}{M^*_{\mathrm{obs}}(2\pi)}\frac{M^*_{\mathrm{obs}}(\pi^0\gamma\gamma)}{M^*_{\mathrm{obs}}(2\pi^0)}\times\left[\frac{\epsilon^*(2\pi^0)}{\epsilon(2\pi^0)}\frac{\epsilon_{2\pi}(\pi^0\gamma\gamma)}{\epsilon^*_{2\pi}(\pi^0\gamma\gamma)}\right]. \tag{11}$$

Without any Monte Carlo calculation, we would expect the bracketed term in Eq. (11) to be close to unity since it involves ratios of detection efficiencies for the *same* process but only different TOF. Indeed, the Monte Carlo calculation of the term in brackets yields the value 1.12. Thus $T_{2\pi}$ calculated from Eq. (11) depends primarily on the observed quantities $M^*_{\mathrm{obs}}(\pi^0\gamma\gamma)$, $M^*_{\mathrm{obs}}(2\pi)$, and $M_{\mathrm{obs}}(2\pi)$, and is relatively independent of the Monte Carlo program. Its value (see Sec. IV) is consistent with that calculated from Eq. (7).

F. Measurement of $R_{\pi\gamma}$

Once R is determined, we can estimate the partial rates for the dominant decays $\eta^0\rightarrow 3\pi^0$ and $\eta^0\rightarrow 2\gamma$ from the observed distribution of γ-ray multiplicities (Table III). Essentially, we use the numbers of two, five, and six γ-ray pictures in the region of the η peak. We make background corrections (for $2\pi^0$ processes, $3\pi^0$ processes, and non-hydrogen events) from observations in the off-peak regions. Using the Monte Carlo results (Table I), we find the rates which best fit these observed multiplicities. $R_{\pi\gamma}$ is then obtained as the ratio of these rates, i.e., $R_{\pi\gamma}=(\eta^0\rightarrow 3\pi^0)/(\eta^0\rightarrow 2\gamma)$.

Since in this experiment we only "detect" η particles which decay through neutral modes, we obtain no direct information about the ratio of the above rates (R and $R_{\pi\gamma}$) to those of the charged modes.

IV. RESULTS

We examined a total of some 25 000 event pictures. For these, there were 1022 which showed four and only four γ-ray showers, and in which there was no indication of γ detection in the shower counter. In addition, these pictures satisfied the criteria of single-pion beam tracks and no malfunction of the spark chambers, etc.

Of these 1022 events, 786 satisfied the preliminary criteria necessary for kinematic reconstruction. (This empirical factor 786/1022 is included, as mentioned earlier in the figures given in Table II for the over-all efficiencies. It does not, of course, enter into the calculation of R when the comparison method, Eq. (3) [or Eq. (6)], is used.) Of these 786, 446 had neutron TOF in the η^0 peak and 340 in the off-peak region.

Table V displays some of the pertinent numbers relating to the values obtained for $M_{\mathrm{obs}}(\pi^0\gamma\gamma)$, $M^*_{\mathrm{obs}}(\pi^0\gamma\gamma)$, $M_{\mathrm{obs}}(2\pi^0)$, and $M^*_{\mathrm{obs}}(2\pi^0)$. Row 1 gives the number of

TABLE V. Number of events which survive each major selection criterion.

Hypothesis Neutron TOF region	$\eta^0\rightarrow\pi^0\gamma\gamma$ η peak	$X^0\rightarrow\pi^0\gamma\gamma$ off peak	$\pi^-+p\rightarrow n+2\pi^0$ η peak	$\pi^-+p\rightarrow n+2\pi^0$ off peak
(1) Pass zero-constraint fit	94	143	94	143
(2) Satisfy $\gamma\gamma$ effective-mass criterion	22	62	15	45
(3) Satisfy all additional criteria	$4=M_{\mathrm{obs}}(\pi\gamma\gamma)$	$12=M^*_{\mathrm{obs}}(\pi\gamma\gamma)$	$5=M_{\mathrm{obs}}(2\pi)$	$17=M^*_{\mathrm{obs}}(2\pi)$

four-γ-ray pictures for which the zero-constraint fit gives four positive energies; row 2 gives the number of these which satisfy the appropriate $\gamma\gamma$ effective-mass criteria; and row 3 gives the number which also satisfy the additional criteria listed in Sec. III. Row 3 also represents the final values of the M_{obs}.

The last term in Eq. (6), evaluated via Eq. (7) using the data in Tables II and IV, equals 0.148. The same term evaluated via Eq. (11) equals 0.233. We have used the average of these two values. Using this average and the numbers from Tables II, IV, and V, we calculate $M_{\text{BGD}}(\pi^0\gamma\gamma)$ from Eq. (5). Finally, R is obtained by substituting this value of $M_{\text{BGD}}(\pi^0\gamma\gamma)$ into Eq. (3). The result is

$$R=-0.027\pm0.070\,, \tag{12}$$

where the uncertainty here is statistical only and comes primarily from the small value of $M_{\text{obs}}(\pi^0\gamma\gamma)$. Sources of possible systematic error have been investigated in detail[6] and are believed to be small compared to the statistical uncertainty. The above result is clearly consistent with a zero value for R. We can express a probable upper limit for R as

$$R\leq 0.07\ (90\%\ \text{confidence}). \tag{13}$$

Assuming a zero contribution from the $\pi^0\gamma\gamma$ decay mode, we can proceed to estimate the rates for the decays $\eta^0\to 3\pi^0$ and $\eta^0\to 2\gamma$. We obtain the result

$$R_{\pi\gamma}=(\eta^0\to 3\pi^0)/\eta^0\to 2\gamma)=0.75\pm0.07\,,$$

the error here being purely statistical. An estimate of the Monte Carlo uncertainty modifies this result to

$$R_{\pi\gamma}=0.75\pm0.09. \tag{14}$$

V. CONCLUSIONS

Our result for R is in good agreement with the work of Baltay *et al.*,[9] Bonamy and Sonderegger,[10] Buniatov *et al.*,[11] and Jacquet *et al.*[12] The evidence presented by these papers as well as our own suggests a very small branching ratio for $\eta^0\to\pi^0\gamma\gamma$ consistent with theoretical expectations. Our measurement of $R_{\pi\gamma}$ is consistent with the world average of 0.72 ± 0.05.[3] The results of this measurement are

Decay channel	Branching fraction (of neutrals)
$\eta^0\to 2\gamma$	0.57 ± 0.03
$\eta^0\to 3\pi^0$	0.43 ± 0.03
$\eta^0\to\pi^0\gamma\gamma$	≤ 0.07 (90% confidence level upper limit)

ACKNOWLEDGMENTS

It is a pleasure to acknowledge the help and assistance of the AGS staff, in particular Dr. James Sanford, Tom Blair, and Jerry Tanguay. The efforts of the entire staff of Nevis Laboratory are gratefully acknowledged, with special thanks to Dennis Yang, our mechanical design engineer. We would also like to thank Dr. W. Lee and colleagues for the use of their neutron counters. We are indebted to the scanning and measuring staffs of Nevis and of Syracuse University, whom we gratefully thank.

[9] C. Baltay, P. Franzini, J. Kim, R. Newman, N. Yeh, and L. Kirsch, Phys. Rev. Letters **19**, 1495 (1967).

[10] P. Bonamy and P. Sonderegger, in *Proceedings of the Heidelberg International Conference on Elementary Particles, Heidelberg, 1967*, edited by H. Filthuth (North-Holland, Amsterdam, 1968).

[11] S. Buniatov, E. Zavatini, N. Deinet, H. Müller, P. Schmitt, and H. Staudenmaier, Phys. Letters **25B**, 560 (1967).

[12] F. Jacquet, U. Nguyen-Khac, C. Baglin, A. Bezaguet, B. Degrange, R. J. Kurz, P. Musset, A. Haatoft, A. Halsteinslig, and J. M. Olsen, Phys. Letters **25B**, 574 (1967).